Marine Geology 480 (2025) 107469

Contents lists available at ScienceDirect

Marine Geology

journal homepage: www.elsevier.com/locate/margo

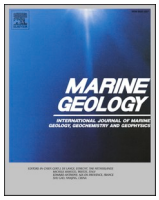

Turbidity current flow structure and its modulation by contour currents: Insights from 3D flume experiments

P.H. Adema [a,*], J.T. Eggenhuisen [a], J. Bleeker [a], R. Silva Jacinto [b], E. Miramontes [c,d]

[a] Faculty of Geosciences, Utrecht University, 3584, CB, Utrecht, the Netherlands
[b] Ifremer, Geo-Ocean, UMR 6538 Plouzané, France
[c] MARUM-Center for Marine Environmental Sciences, University of Bremen, Bremen 28359, Germany
[d] Faculty of Geosciences, University of Bremen, Bremen 28359, Germany

ARTICLE INFO

Editor: Michele Rebesco

Keywords:
Turbidity currents
Contour currents
Combined flow
Mixed depositional systems
Secondary flow

ABSTRACT

Turbidity currents are the main agent transferring sediment, carbon, nutrients and pollutants (e.g. micro-plastics) from the continents to the deep sea. They flow through submarine canyons, connecting the continents to the oceans. Along their trajectory, these flows may interact with a suite of oceanographic processes, such as geostrophic contour currents, forming a mixed system, entraining material from the turbidity current into the large-scale ocean system. Turbidity current–contour current interaction is scarcely evaluated and their combined three-dimensional flow structure is poorly constrained. We conducted experiments showing the 3D flow structure of turbidity currents and how this structure is modified by contour currents for different contour current velocities, channel depths, and morphologies. Secondary flow cells are observed in the experimental turbidity currents inside the straight channel. This secondary flow is bi-cellular for the purely gravity-driven experiments. Contour currents collapse this bi-cellular structure into a single cell constrained to the downstream channel margin. Additionally, the contour currents modulate the overspilling behavior of the flow by reducing overspill on the upstream overbank and making overspill thicker and faster on the downstream overbank. Our results illustrate the importance of secondary circulation in turbidity currents and their structural modulation by contour currents.

1. Introduction

Turbidity currents are geophysical flows that flow down submarine canyons due to gravity acting on sediment that is suspended in the flow. They are the primary process transferring sediment (Covault et al., 2011; Talling et al., 2015), terrestrial organic carbon (Galy et al., 2007; Talling et al., 2024), nutrients (Canals et al., 2006), and pollutants such as (micro)plastics (Pierdomenico et al., 2020, 2023; Pohl et al., 2020) from the continents to the deep sea. Interactions and exchanges between downslope turbidity currents and along-slope contour currents are common (Fuhrmann et al., 2022; Miramontes et al., 2020; Rodrigues et al., 2021; Shanmugam et al., 1993). Such ocean processes entrain materials from turbidity currents (Kane et al., 2020; Rodrigues et al., 2022), exporting them away from the down-slope fairway to build continental slopes, which are archives of the Earth's climate and ocean circulation. For instance, the advection of silt-sized sediment from the top of turbidity currents is a source mechanism for the widely applied sortable silt proxy to reconstruct the strength of the thermohaline circulation (Bianchi and McCave, 1999; McCave et al., 1995). Furthermore, contour currents efficiently convey nutrients and oxygen, which sparks bio-diversity (Hebbeln et al., 2016; Henry and Roberts, 2007). Through their interaction with turbidity currents, contour currents therefore effectively connect terrestrial sources of plastic pollution to these biodiversity hotspots, which poses a threat to the biota living in these ecosystems (Kane et al., 2020). Thus, entrainment and exchange between turbidity currents and contour currents is pivotal in understanding their significance to the larger ocean system.

The flow- and sediment dynamics of combined turbidity current–contour current systems are a topic of active dispute in the literature. Some authors emphasize that contour currents interact with the very top of turbidity currents, advecting sediment out of the channel in elevated plumes that deposit sediment in the interchannel areas (Shanmugam et al., 1993) (Fig. 1A). Other studies suggest that oscillations of the density interface (Gong et al., 2018) or secondary

* Corresponding author.
E-mail address: p.h.adema@uu.nl (P.H. Adema).

https://doi.org/10.1016/j.margeo.2024.107469
Received 20 June 2024; Received in revised form 8 November 2024; Accepted 26 December 2024
Available online 28 December 2024

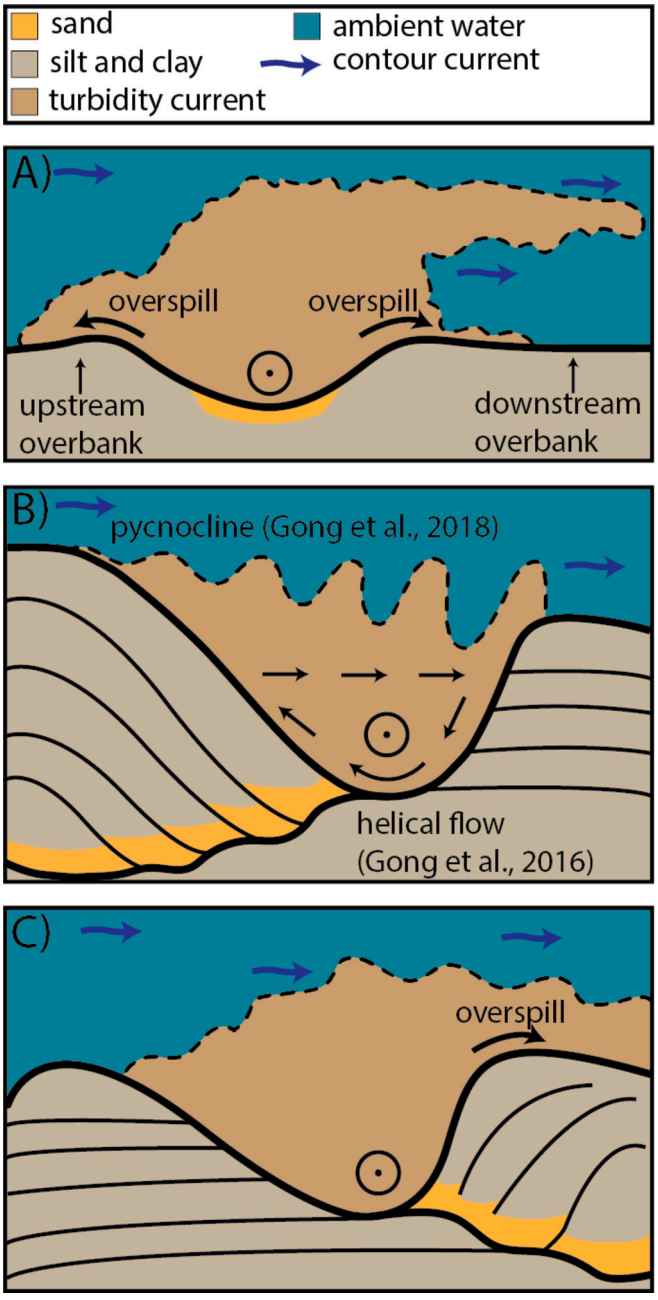

Fig. 1. Conceptual models of mixed turbidity current-contour current flow proposed by previous studies A) Shanmugam et al. (1993), B) Gong et al., (2016, 2018) C) Chen et al., (2020), Fonnesu et al. (2020), Fuhrmann et al. (2020). The upstream overbank and downstream overbank are identified relative to the contour current flow direction.

circulations (Gong et al., 2016) cause erosion on the downstream channel margin, causing the channels to migrate in the contour current direction (Fig. 1B). Contrastingly, asymmetric overspill and deposition of sediment onto the downstream levee have also been suggested to dominate, causing channels to migrate against the contour current direction (Fig. 1C) (Chen et al., 2020, 2024; Fonnesu et al., 2020; Fuhrmann et al., 2020). One reason for the lack of clarity in this debate is that it is unclear how the combined 3D flow structure of turbidity currents and contour currents governs the exchange of sediment between the channel and the slope.

In this study, we consider the case of synchronous interaction between gravity flows and contour currents that forms a combined flow field (Fonnesu et al., 2020). Studies on flow fields in open-channel flow and pipe flow show that secondary circulation is a common feature in channelized flow (Imamoto and Ishigaki, 1992; Oertel, 2010). While an extensive body of literature treats secondary circulation in channelized gravity flows forced by channel curvature (Azpiroz-Zabala et al., 2017a; Corney et al., 2006; Imran et al., 2007; Keevil et al., 2006; Sumner et al., 2014) and the Coriolis effect (Cossu et al., 2015; Cossu and Wells, 2010; Wells and Cossu, 2013), the across-channel velocity structure of overspilling turbidity currents in absence of such orthogonal forcing is wholly unknown. Therefore, we first present 3D flume-tank experiments that identify the intrinsic flow structure of turbidity currents in a straight channel by measuring multiple profiles of 3D velocity across a channel cross-section. This approach allows us to identify 3D flow structures such as secondary flows and measure the channelized and the overspilling parts of the flow. Secondly, we study the modification of this structure by contour currents. We vary the contour current intensity, the channel depth and the channel (a)symmetry, to test the applicability of the previously suggested models for a range of conditions. We show that turbidity currents intrinsically form a stable bi-cellular circulation, similar to secondary circulation in free-surface flows. In combined flows the bi-cellular structure collapses and a single cell is constricted to the downstream channel margin.

2. Materials and methods

2.1. Experimental set-up

The experiments were conducted in the Eurotank Flume Laboratory in Utrecht, the Netherlands. The Eurotank is an 11x6x1.2 m basin (LxWxD) (Fig. 2) in which turbidity current experiments (de Leeuw et al., 2018a, 2018b; Pohl et al., 2019), combined flow experiments (Miramontes et al., 2020), and contour current experiments (Wilckens et al., 2023) were conducted previously. The basin contained a 5-degree slope with a preformed, 80-cm wide, symmetrical channel made of poorly sorted coarse sand which is not suspended in the flow (Fig. 2A and B). Values of experimental parameters are reported in Table 1.

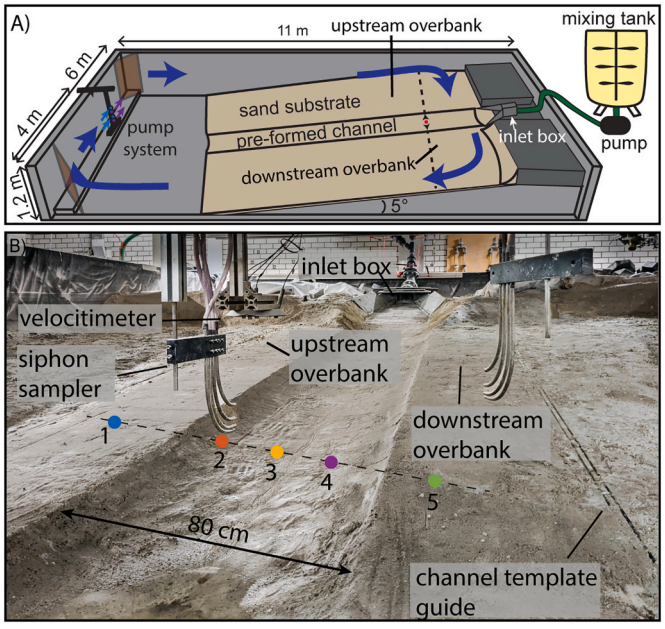

Fig. 2. A) Schematic drawing of the experimental set-up. The red dot is the central position of the velocimeter. B) Photo of the experiment showing the siphon samplers used for concentration measurements, the velocimeter, and the channel. Colors in numbers in B indicate stopping positions for the velocimeter and correspond to velocity profiles in Fig. 3. (For interpretation of the references to colour in this figure legend, the reader is referred to the web version of this article.)

Table 1
Experimental parameters and boundary conditions of the experiment.

Parameter	Value	Unit
Grain size	0.4–200	μm
Modal grain size input	63	μm
$\rho_{sediment}$	2300	kg m^{-3}
ρ_{bulk}	1085	kg m^{-3}
Mixer volume	900	L
Discharge	6.4	L s^{-1}
Slope	5	degrees
Channel width	80	cm
Channel depth	4 or 7 or 10	cm

First, 145 kg sediment (0.4–200 μm, mode = 63 μm, ρ = 2300 kg m^{-3}) was mixed with 845 L water in a ~ 900 L mixing tank, creating a homogenized suspension with a density of 1085 kg m^{-3}. Second, the mixture was pumped at a constant discharge of 6.4 L s^{-1}, monitored by a discharge meter. The mixture was released underwater into the channel from where it flowed downslope by gravity, forming a turbidity current. Pumps were used to drive a recirculation in the tank, which acts as an analogue to a geostrophic contour current (Wilckens et al., 2023). A two-pump set-up (Fig. 2A) allowed us to create both a weak contour current (1 pump) and a strong contour current (2 pumps), resulting in depth-averaged along-slope velocities of 4 and 7 cm s^{-1} respectively, above the channel axis (Fig. 2B and C). The pumps were mounted on the short wall of the flume and pumped water perpendicular to the channel. Deflection of the flow by diagonally placed sheets of plywood and the walls guided the water around to flow in a vortex (Fig. 2A and 3B). The channel depth was set at 4, 7, and 10 cm. Aspect ratios of the channels are 20, 11.4 and 8 respectively (Table 2). Channel asymmetry was created in two experiments by partly filling the space between one of the channel margins and the channel axis with sand, which created one bank with a gentler slope. The asymmetry is based on published seismic lines of mixed turbidite-contourite-system channels such as in the Lower Congo Basin (Gong et al., 2018) or the Mozambique Channel (Miramontes et al., 2021). We tested two cases of asymmetry: the steep bank facing the contour current and the gentle bank facing the contour current. The asymmetrical experiments were only run for the weak contour current to focus on the interaction between the combined flows and the morphology. This study reports on 7 experiments in total (Table 2).

2.2. Data acquisition

We measured a channel–cross-section of the combined flow field. Flow velocities were recorded in 3D with a UDOP4000 (www.signal-processing.com) using pulsed ultrasound Doppler velocimetry (device settings in Supplement, Table S1). This device uses 1 emitter probe with 3 receivers (Supplement, Fig. S1). This configuration is different from 1D Doppler techniques commonly used in the laboratory; it allows a vertical profile of 3D velocity to be measured, with the 3D-directions correlated in time at each elevation. 1 MHz probes were used with a vertical resolution of 0.9 mm. A pilot experiment with the velocimeter fixed in the center of the channel determined that a steady phase lasted ~110 s (Fig. 3A). The velocimeter was moved to five locations across the channel during the steady phase of each subsequent experiment, measuring the flow field at three locations in the channel and at one location on each overbank area. The velocimeter was vertically positioned 23 cm above the bed on the overbanks. Velocities were time-averaged at each locality using 10-s windows. The symmetrical channel experiments were sampled for sediment concentration with siphon samplers inside the channel and on the downstream overbank. The samplers consisted of 4 tubes each, mounted at 1, 2, 4, and 8 cm above the bed (Fig. 2B).

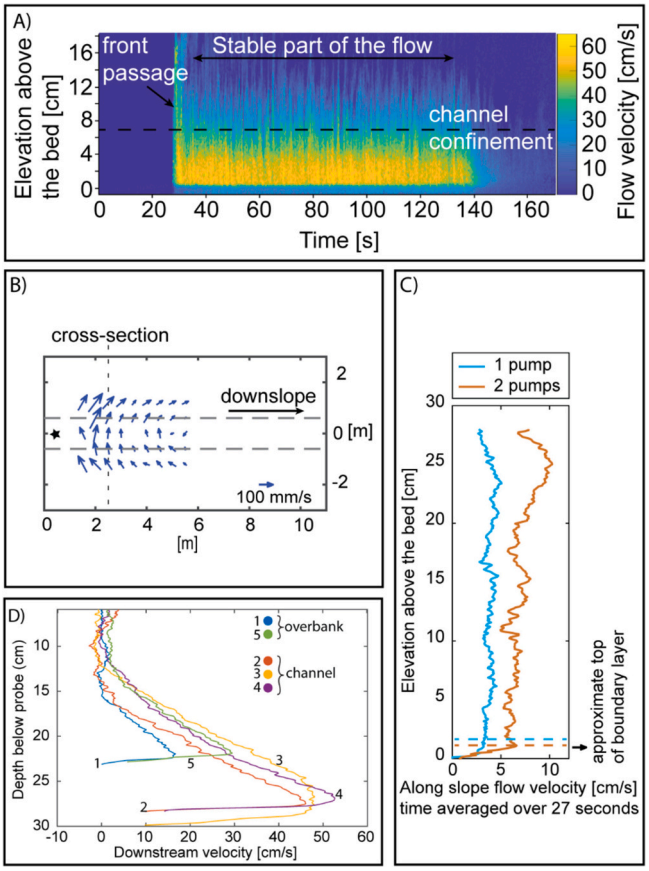

Fig. 3. A) Time series of a pilot experiment without a turbidity current determining the stability of the experiment. This test run had the velocity probes fixed in the center of the channel, boundary conditions are the same as in experiment 2. B) Measured contour current flow field for the strong contour current case (2 pumps). The black star marks the entry point for the sediment gravity flow in the channel. C) Contour current velocity profiles for tests with only a contour current, the measuring position is in the channel center at 2.50 m. Time-averaged contour current boundary layer thicknesses are indicated with the dashed lines. D) Velocity profiles of the down-slope component of the velocity for the experiment with 1 contour current and a 7 cm deep channel (Experiment 3/Fig. 4B).

2.3. Flow scales

2.3.1. Contour currents

In nature, contour currents result from a geostrophic equilibrium, where the flow velocity is orthogonal to the pressure gradient and to Coriolis on the opposite side. (Heezen et al., 1966). In our flume, we cannot scale down the Coriolis effect because the tank does not rotate within the laboratory, as is the case in experiments that account for this effect (Cossu et al., 2015; Wells and Cossu, 2013). Scaling the geostrophic current using the Rossby number is therefore not possible. Instead, we set up a radial acceleration by making the contour current flow in circular motion along a curved slope. The flow field of the circulatory flow was measured by measuring the flow without a turbidity current present (Fig. 3B). This circulatory current acted as an analog for naturally occurring geostrophic contour currents flowing parallel to the slope (Wilckens et al., 2023). The depth-integrated contour-current flow velocities of our experiments were 4 and 7 cm s^{-1}, which we refer to as weak and strong in this paper. Time-averaged velocity profiles for the contour current show boundary layer thicknesses of 1–2 cm respectively (Fig. 3C).

Table 2
List of experiments, boundary conditions and flow scales. All other experimental parameters were the same for all experiments (Table 1). Asymmetrical 1 is the experiment with the steep bank facing the contour current, Asymmetrical 2 is the experiment with the gentle bank facing the contour current (Fig. 5). Bulk densimetric Froude numbers inside the channel were calculated using the Ellison and Turner integrals following Sequeiros et al. (2010), based on concentration profiles in Fig. 4. The flow depth is depth-integrated and follows from the method described in Ellison and Turner (1959).

Run #	Channel depth (D) [cm]	Channel aspect ratio Width:height [−]	Contour current [cm s^{-1}]	Flow Depth (h) [cm]	Channel shape	Dimensionless vertical scale [−] $\frac{Flow\ depth\ [m]}{Channel\ depth\ [m]}$	Froude number [−]
1	4	20	4	0.13	Symmetrical	3.3	1.9
2	7	11.4	0	0.12	Symmetrical	1.7	2.5
3	7	11.4	4	0.13	Symmetrical	1.9	1.9
4	7	11.4	7	0.16	Symmetrical	2.3	1.9
5	10	8	4	0.16	Symmetrical	1.6	1.6
6	7	11.4	4	0.14	Asymmetrical 1	2.0	–
7	7	11.4	4	0.13	Asymmetrical 2	1.9	–

2.3.2. Turbidity currents

Flow scales for the turbidity currents are based on the concentration profiles and on the downslope component of the velocity data. Sediment concentration profiles were fitted through the combined channel and downstream overbank concentration data using a 2-parameter exponential model (Garcia, 1994; Sequeiros et al., 2010). Concentrations near the bed are around 6 vol%, decreasing to 0 vol% at the top of the flow (Fig. 4). We calculated scales for the flow depth and depth-averaged values for velocity and concentration from these measured profiles, following Ellison and Turner (1959) and used these to compute the downslope component of the bulk densimetric Froude number in the channel as described in (Sequeiros et al., 2010). Froude numbers range from 1.6 to 2.5 with a mean value of 2.0 showing that the flows are supercritical (Table 2). The vertical scale of the flows is non-dimensionalized by dividing the depth-integrated flow depth (h) arising from the evaluation of the integrals (Ellison and Turner, 1959), by the channel depth (D) (flow depth/channel depth) (Table 2). This parameter quantifies the degree of effective confinement of the flow in the channel with lower numbers indicating better confinement. Mohrig and Buttles (2007) showed experimentally that flows with h/D ratios of 1.3 and lower can be considered fully channelized, resulting in downslope velocities up to an order of magnitude higher than the across-channel overspill velocities. If $1.3 < h/D \leq 5$ flows are quasi-channelized and for $h/D > 5$ flows are unconfined. Dimensionless vertical scales for our experiments range between 1.6 and 3.3, classifying them as quasi-confined flow following the conditions of Mohrig and Buttles (2007) (Table 2).

2.3.3. Combined flow

Scaling of the combined flow requires understanding of the processes that govern the flow interaction. Yet, there are no in-situ measurements of combined flow, so the literature provides no guidance on how the interaction between turbidity currents and contour currents should be scaled. We therefore take a pragmatic approach and initially compare the relative velocities of the turbidity current and the contour current (Miramontes et al., 2020). This choice is substantiated by the self-similar scaling of plane mixing layers by the velocity difference across such structures (Champagne et al., 1976; Pope, 2000). Turbidity currents in natural systems typically have velocities ranging from a few decimeters to several meters per second (Azpiroz-Zabala et al., 2017a, 2017b; Gavey et al., 2017; Khripounoff et al., 2012; Xu et al., 2004). Contour currents flow at more gentle speeds, usually not exceeding several tens of cm per second (Shanmugam et al., 1993; Miramontes et al., 2019; Sánchez-Leal et al., 2017; Wilckens et al., 2021; Zhao et al., 2024). The two contour current velocities of 4 and 7 cm s^{-1} correspond to 8 and 14 % of the downslope velocity maximum (~50 cm s^{-1}), respectively. This range of ratios is in line with field measurements of the two processes (Fuhrmann et al., 2022).

3. Results

3.1. Influence of contour current intensity

In the absence of contour currents, the turbidity currents in the experiments overspilled nearly symmetrically on both sides of the channel (Fig. 4A). The down-slope-oriented velocity core flowed up to 52 cm s^{-1} and was located at the channel axis. The flow in the 7 cm deep channel was quasi-channelized with an h/D value of 1.7, 1.9 and 2.3 for the no contour current, weak contour current, and strong contour current case respectively (Table 2). A bi-cellular secondary circulation established, which flowed inward at bed-level from both sides of the channel and outward above the confinement of the channel. Circulation cells rotated in opposite directions with the center of the two cells being slightly offset to the side of the channel axis (Fig. 4).

When a contour current was added to the experiment, the combined flow field differed substantially (for the velocity profiles see Fig. 2D). Increasing contour current intensities resulted in stronger asymmetry in the combined flow structure (Fig. 4B and C). With the weak contour current, overspill was reduced relative to purely turbiditic experiments and a stationary lateral front formed on the upstream overbank (Fig. 4B). The strong contour current blocked the upstream overbank overspill completely (Fig. 4C). On the downstream overbank, overspill was thicker when contour currents were present. Furthermore, downslope-flow velocities were faster with than without a contour current on the downstream overbank. The downstream velocity maximum was 48 cm s^{-1} for both contour current settings. The bi-cellular circulation observed with the turbidity current alone (Fig. 4A) was absent in the combined flow. The upstream cell collapsed when the weak contour current was added. A single circulation cell formed downstream of the channel axis (Fig. 4B). The strong contour current amplified this result, further displacing the cell downstream and decreasing its size and flow velocity (Fig. 4C).

3.2. Influence of channel depth

Three different channel depths were used in combination with the weak contour current (Fig. 4D–F). For all channel depths, overspilling occurred on both sides of the channel, with reduced overspilling for the deeper channels. Effective confinement (h/D) ranged from 3.3 for the shallow channel to 1.9 and 1.6 for the intermediate and deep channel respectively. Overspilling on the downstream overbank is thicker and denser for deeper channels (Fig. 4D–F). The 7 and 10 cm channel experiments had downstream velocity maxima of 53 and 51 cm s^{-1} respectively (Fig. 4D, E and F). For the 7 cm deep channel, the high-velocity core was displaced downstream from the thalweg. However, for the 10 cm deep channel, the velocity core was in the center of the channel. The 4 cm channel (Fig. 4D) experiment had a downstream velocity maximum of 47 cm s^{-1} and did not show a secondary

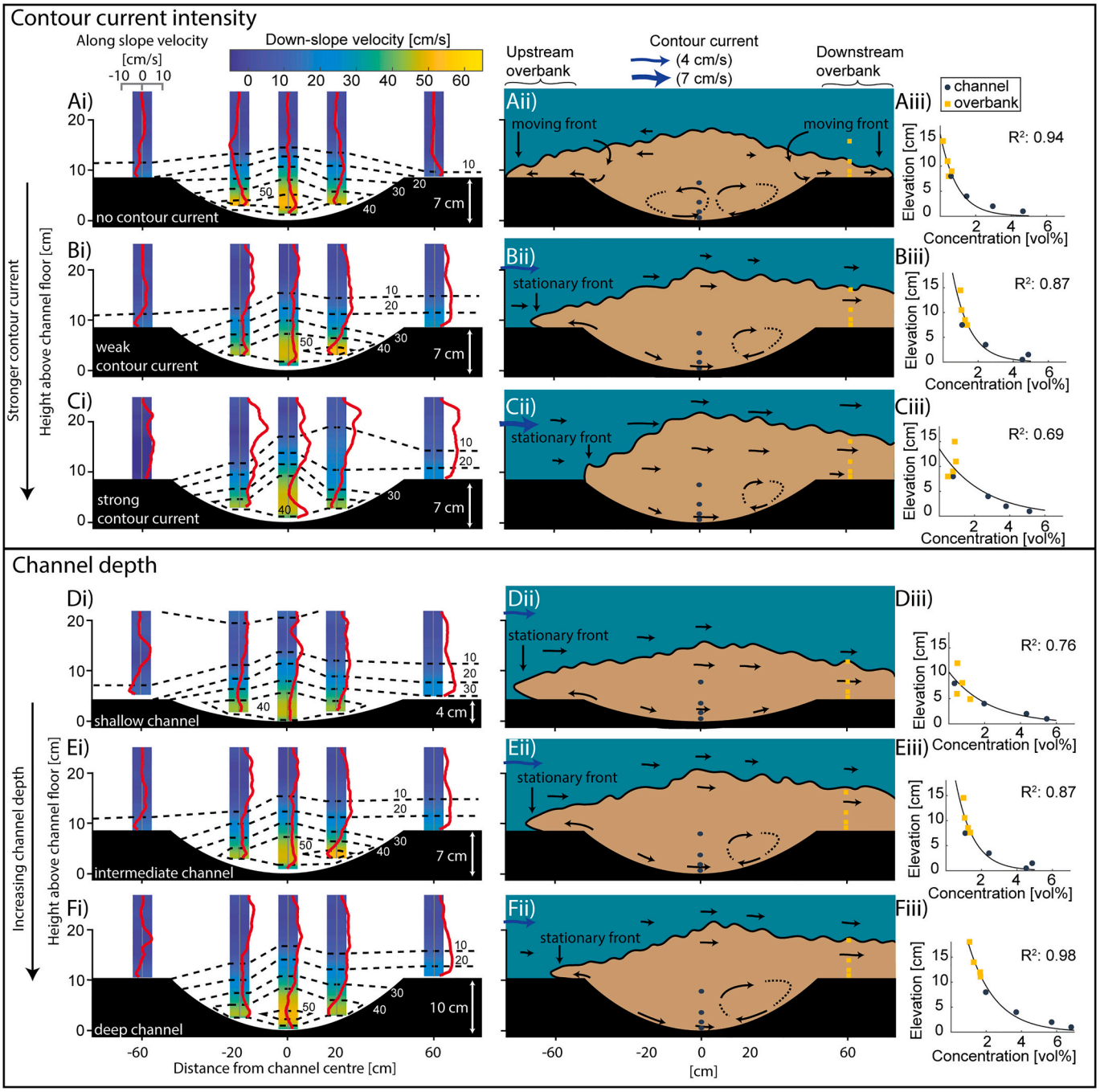

Fig. 4. Contour current intensity experiments (A-C). Channel depth experiments (D-F) with the weak (4 cm s^{-1}) contour current. The upstream overbank and downstream overbank are identified relative to the contour current flow direction. Dark blue circles and yellow squares indicate the positions of siphon samplers. The interpretation of the flow structure is based on a combination of the concentration profiles and the 10 cm s^{-1} contour lines of the down-slope component of the velocity. Channel aspect ratios and dimensionless vertical scales are reported in Table 2. (For interpretation of the references to colour in this figure legend, the reader is referred to the web version of this article.)

circulation cell whereas the 7 and 10 cm channels both did, with the deepest channel generating the largest circulation cell. In both cases, the circulation cell formed downstream of the channel thalweg.

3.3. Influence of channel asymmetry

Our experiments show that the turbidity current has a higher velocity maximum and a larger high velocity core for both cases of asymmetry compared to a symmetric channel of equal depth, despite the asymmetric channel having a smaller cross-section (Fig. 5 vs. Fig. 4B). The velocity maxima are 54 cm s^{-1} (Fig. 5A) and 59 cm s^{-1} (Fig. 5B), compared to 47 cm s^{-1} for the symmetrical equivalent with the same channel depth and contour current velocity (Fig. 4B). Furthermore, the type of symmetry seems to control the cell characteristics. When the steep bank faces the contour current, the circulation cell flows slower than in the symmetrical experiments. When the gentle bank faces the contour current the opposite occurs: the cell becomes larger and faster flowing than in symmetrical experiments.

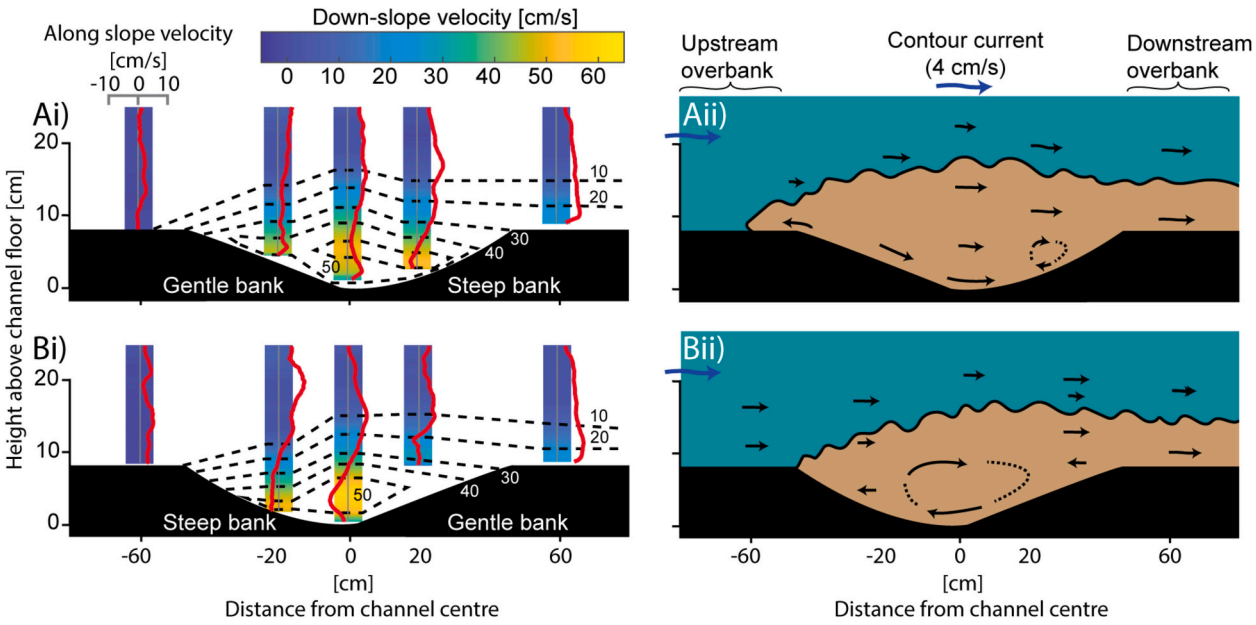

Fig. 5. Experiments testing channel asymmetry. Panel A: the steep bank faces the contour current. Panel B: the gentle bank faces the contour currents.

4. Discussion

4.1. Channel depth and asymmetry

The effective confinement (h/D) was 1.7 (no contour current) and 1.9 and 2.3 for the weak and the strong contour current case respectively (Fig. 4B and C vs. 4A), indicating lower effective confinement (higher h/D) for higher contour current velocities. The flow depth (h) increases because of blocked overspill by the contour current on the upstream overbank, creating a thicker current in the center of the channel and promoting overspill to the downstream overbank by advection from the flow by the contour current. Furthermore, the effective channelization of our experiments increases with increasing channel depth (Table 2. Run 1, 3 and 5). The least channelized experiment was the 4 cm channel depth experiment (Table 2. Run1) with a h/D value of 3.3. The 7 cm and 10 cm channels had h/D values of 1.9 and 1.6 respectively. This is in line with findings from studies treating channel overspill (de Leeuw et al., 2018a, 2018b; Mohrig and Buttles, 2007) in the sense that deeper channels result in stronger effective channelization generating less overspill onto the overbanks and yield lower along-slope flow velocities relative to the downslope velocity (Fig. 4). However, for combined flows the contour current–induced modulation of the effective confinement has an additional effect. Channel confinement governs the degree of interaction between turbidity currents and contour currents. Along the turbidity current–contour current interface a mixing layer forms which thickens from the point where the two flows first meet towards the downstream overbank. This affects the mixing dynamics of combined flows.

The Froude number is often referred to as a measure of mixing between turbidity currents and the ambient, with higher Froude numbers indicating more mixing because of higher shear at the top of the flow relative to the restoring buoyancy forces (e.g. Sequeiros, 2012). However, the bulk Froude number alone is not enough to parameterize the mixing of turbidity currents and combined flows with varying channel depths. Table 2 shows that runs 1, 3 and 4 have a Froude number of 1.9 while having h/D ratios of 3.3, 1.9 and 2.3 respectively. Despite the Froude number being the same for these flows, the effective channelization (h/D) is not. The effective channelization affects the interaction with the ambient, so we argue that h/D should be considered as well when parameterizing mixing. Furthermore, the degree of confinement modulates how the contour current affects the stratification inside the channel. Comparison of the sediment concentration profiles of the shallow and the intermediate channel (Fig. 4D vs. 4E) shows that the top two channel siphon samples for the intermediate channel are denser than for the shallow channel but the 2 siphon samples close to the bed are not. Comparing the shallow channel with the deep channel (Fig. 4D vs. 4F) shows that all deep channel siphon samples have higher concentrations than their low confinement counterparts.

In the shallowest channel (h/D = 3.3) (Fig. 4D), no cellular flow on a scale similar to cells in the deeper channels was observed. In the deeper channels, a single secondary circulation cell formed that was larger when the channel depth increased (Fig. 4E and F). The channel-scale secondary circulation in combined flow proposed by (Gong et al., 2016) thus seems most likely in partially- to well-confined flow, and not in poorly confined flow.

Asymmetrical channels prevent overspilling on the upstream overbank even with the weak contour current (Fig. 5), contrary to a symmetrical channel with the same contour current (Fig. 4B). Moreover, asymmetrical channels accommodated the fastest maximum downstream velocities in all our experiments, with larger high-velocity cores. Channel asymmetry thus promotes the effectiveness of flow of combined contour current–turbidity current flow and has effects that are similar to increasing channel depth in symmetrical channels. The orientation of the asymmetry affected the size of the flow cell, which is in line with findings from the Strait of Bosphorous (Black Sea) that show that channel shape and topography are important in controlling the structure of flow cells in submarine channels (Sumner et al., 2014).

4.2. Secondary circulation in turbidite channels

All our experiments except the 4 cm deep channel (Fig. 4D) show secondary circulation cells. Circulation-cell formation has been treated for channelized turbidity currents in meander bends (Azpiroz-Zabala et al., 2017b; Corney et al., 2006; Cossu and Wells, 2010; Imran et al., 2007; Keevil et al., 2006), invoking processes such as lateral stratification, superelevation, centrifugal forces and Coriolis. Secondary circulation is also thought to occur in straight channels, resulting from contour-current-induced superelevation of the gravity flow towards the steep bank (Gong et al., 2018) or for the head of the flow during cleft structure formation (Simpson, 1972). Our experiments show a bi-cellular circulation in a straight channel within an a priori symmetrical environment, i.e. independent of meandering, Coriolis, or

interaction with contour currents (Fig. 4A). The two cells form adjacent to each other with their flows converging near the channel center at bed level and flowing outward at the top. This sense of rotation is opposite to the reported bi-cellular circulation in a fully confined turbidity current in a straight channel as reported by Cossu and Wells (2010). This can be explained by the fact that their experiments were fully confined whereas the flows in this study were affected by channel overspill. We suggest that two processes may contribute to the measured circulation: laterally heterogeneous turbulent mixing and overspilling.

While laterally-adjacent bi-cellular flow in straight channels are rarely discussed in the context of turbidity currents, they are a classic result in hydraulic engineering studies with turbulent open-channel flow (Einstein and Li, 1958; Hwang and Lee, 2018; Nezu and Nakagawa, 1984; Shiono and Knight, 1991). Flume experiments with open channels (Nezu and Nakagawa, 1984), closed ducts (Knight and Patel, 1985), and compound channels (Imamoto and Ishigaki, 1992) showed that secondary flows are a recurrent feature in turbulent flows and are related to heterogeneity in the shear-stress distribution in the channel. Variations of the secondary flow occur depending on the channel morphology, aspect ratio, and modulation by a free surface.

Our experiments have curved channel floors. The decrease in depth away from the center up to the overbanks creates a heterogeneous distribution of relative roughness (r), which is inversely proportional to flow depth (h) and proportional to absolute roughness (K) (Hinsberger et al., 2022; Shiono and Knight, 1991):

$$r = \frac{K}{h} \tag{1}$$

Consequently, the flow goes faster in the center of the channel than on the sides. This creates a lateral velocity gradient superimposed on the vertical velocity gradient, forming a lateral shear zone (Fig. 6). In this shear zone, vortices with vertical axes form. These vortices transfer mass and momentum from the channel center to the sides (Shiono and Knight, 1991). Because of the reversal of the velocity gradient at the top of the boundary layer in turbidity currents, vorticity-induced momentum and mass transfer to the sides are largest at the top of the boundary layer and smaller near the bed. This is in contrast to open channel flows without velocity gradient reversals, where the vorticity is set up near the free surface. Continuity requires the transfer of mass at the top of the boundary layer to be balanced by an inward-directed flow at bed level (Fig. 4A-C, E, F; Fig. 6). The resulting circulation cell classifies as a Prandtl type 2 cell because anisotropy of turbulence is its generative mechanism. The resulting flow structure is double helicoidal, with convergent flow at the thalweg near the bed (Fig. 6).

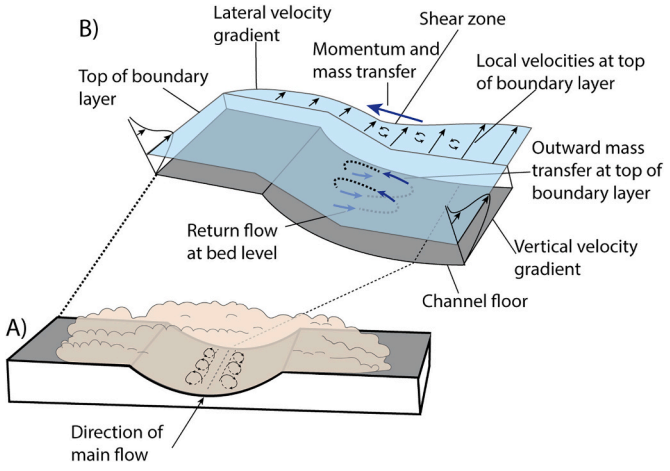

Fig. 6. 3D flow model of the full channel cross-section (A) and half the cross-section (B) zooming in on the dynamics around the boundary layer. Based on Shiono and Knight, 1991.

However, this mechanism would require maximum outward-directed lateral flow velocity at the top of the boundary layer. While the outward-directed flow maximum in our experiments extends well above the boundary layer, suggesting this process may only account for part of the observations.

Additionally, outward-directed flow can be induced by overbank flow. Without contour currents, the flows are thicker in the channel center than on the overbanks. This creates a pressure gradient that is counteracted by the slope of the channel margins, pushing the flow back into the channel. If the flow and the channel are not in equilibrium, overspilling occurs, resulting in outward-directed flow that is strongest above the channel confinement. Continuity requires this overspilling to be balanced by a decrease in current height, where the flow is tuned to the channel or by entrainment of ambient water into the flow (Kelly et al., 2019). The size of the cells compared to the boundary layer thickness of the flow suggests that overspilling drives outward-directed flow velocities in the circulation cells above the upper limit of the boundary layer. This allows the circulation cells to extend above the boundary layer.

When a contour current is added to a turbidity current, the bi-cellular structure collapses. A single cell is maintained downstream of the channel axis (Fig. 4B and C). We think that the asymmetry of the combined-flow structure results from the uni-directional contour current creating a pressure gradient, interacting with the overspilling turbidity current, which has opposing flow directions across the channel. The upstream cell collapses because the contour current-induced pressure gradient counteracts the overspill, momentum and mass transfer against the contour current direction and starts to dominate the upper part of the flow upstream of the thalweg (Fig. 4B, C, E, F). Whereas on the downstream side of the thalweg, the contour current pressure gradient induces flow from the center to the side with the overspilling direction, so the cell can be maintained. Following the definition by Prandtl Oertel (2010), the combined flow single-cell configuration is a type 1 cell as it is forced by a pressure gradient.

4.3. Implications of our experiments

Generalizations of our experiments to natural systems can be made for flows that have similar geometric scales and flow scales to the ones in our experiment (Section 2.3). Our findings on secondary flow cells have implications for sediment suspension in submarine channel and slope systems. Our experiments suggest that cellular secondary flows develop intrinsically in turbidity currents, and that overspilling is a key controlling process. The analogy with channelized free-surface flows is relevant to understanding secondary flow in turbidity currents. Turbidity currents generate turbulence within highly stratified conditions. The gravity-driven sediment suspension generates both the turbulence and the stratification that may partially dampen the turbulence, while the interaction with the ambient fluid is increased compared to free-surface flows. Secondary flows have long been suggested to affect sediment suspension (Einstein and Li, 1958; Falcini et al., 2014), and therefore play a key role that controls this vertically stratified flow structure. More recently, observations of helical flow cells in meanders in the Congo submarine channel system are suggested to contribute to the across-channel transport of sediment as well as vertical mixing (Azpiroz-Zabala et al., 2017b). Our results support the idea that secondary flow promotes long run-out by mixing sediment upward in the flow. Furthermore, the modulation of the flow structure by contour currents is critical in determining sediment suspension in combined flows. This controls entirely what part of the sediment load (sediment, nutrients, pollutants) is entrained into the ocean system. The flow structures we measured are strongly controlled by the boundary layer thicknesses of the two flows and the scale of the flow relative to the scale of the channel. We suggest that moving forward, these parameters together with the relative flow speeds of the two flows are the important scales to consider when studying mixed systems at various scales.

5. Conclusions

In this study, we show novel results from controlled experiments for supercritical, quasi-channelized, combined turbidity current-contour current flows for varying contour current intensities, channel depths and channel morphologies. Overspilling turbidity currents exhibited a bi-cellular secondary circulation that flowed outwards above the channel confinement and at the top of the boundary layer, and inwards along the bed from the channel margins to the channel thalweg. The contour current and channel morphology had the following main effects. Firstly, in combined flow, the bi-cellular circulation of turbidity currents collapses into a single circulation cell, which is displaced from the channel center in the direction of contour current flow. Secondly, the overspill is blocked on the upstream overbank and thicker on the downstream overbank, with higher downslope velocities on the downstream bank. Thirdly, asymmetrical channels accommodate a larger high-velocity core of the combined flow inside the channel and yield faster maximum downstream velocities than the 7 cm channel depth symmetrical experiment. Together these findings show that contour currents can modify the flow structure of turbidity currents, even when weak compared to turbidity currents. The cellular flow helps to maintain the flow core and sustain the flow. Moving forward, we need to consider mixed systems with a new flow model that differs from the classic turbidity current model. With this model, we can understand what role mixed systems play in building climate archives on continental slopes and in distributing sediment and pollutants in the oceans.

CRediT authorship contribution statement

P.H. Adema: Writing – review & editing, Writing – original draft, Visualization, Validation, Methodology, Investigation, Formal analysis, Data curation, Conceptualization. **J.T. Eggenhuisen:** Writing – review & editing, Supervision, Methodology, Investigation, Funding acquisition, Conceptualization. **J. Bleeker:** Methodology, Investigation. **R. Silva Jacinto:** Writing – review & editing, Supervision, Methodology, Investigation, Conceptualization. **E. Miramontes:** Writing – review & editing, Methodology, Investigation, Conceptualization.

Declaration of competing interest

The authors declare that they have no known competing financial interests or personal relationships that could have appeared to influence the work reported in this paper.

Data availability

All research data published in this work is published and freely accessible at: https://doi.org/10.24416/UU01-TLXAOS under the Creative Commons Attribution 4.0 International Public License.

Acknowledgments

The work presented in this paper was funded by the Dutch Research Council (grant OCENW.KLEIN.462). We are grateful for the technical assistance provided by Han de Witte, Henk Markies, and Marcel van Maarseveen. Constructive comments by Gaetano Porcile and Mathew Wells to a previous version of this manuscript helped us to improve the paper.

Appendix A. Supplementary data

Supplementary data to this article can be found online at https://doi.org/10.1016/j.margeo.2024.107469.

References

Azpiroz-Zabala, M., Cartigny, M.J.B., Sumner, E.J., Clare, M.A., Talling, P.J., Parsons, D. R., Cooper, C., 2017a. A general model for the helical structure of geophysical flows in channel bends. Geophys. Res. Lett. 44, 11,932–11,941. https://doi.org/10.1002/2017GL075721.

Azpiroz-Zabala, M., Cartigny, M.J.B., Talling, P.J., Parsons, D.R., Sumner, E.J., Clare, M. A., Simmons, S.M., Cooper, C., Pope, E.L., 2017b. Newly recognized turbidity current structure can explain prolonged flushing of submarine canyons. Sci. Adv. 3, e1700200. https://doi.org/10.1126/sciadv.1700200.

Bianchi, G.G., McCave, I.N., 1999. Holocene periodicity in North Atlantic climate and deep-ocean flow south of Iceland. Nature 397, 515–517. https://doi.org/10.1038/17362.

Canals, M., Puig, P., de Madron, X.D., Heussner, S., Palanques, A., Fabres, J., 2006. Flushing submarine canyons. Nature 444, 354–357. https://doi.org/10.1038/nature05271.

Champagne, F.H., Pao, Y.H., Wygnanski, I.J., 1976. On the two-dimensional mixing region. J. Fluid Mech. 74, 209–250. https://doi.org/10.1017/S0022112076001778.

Chen, M., Wu, S., Wang, R., Zhang, J., Xie, P., Wang, M., Wang, X., Xiong, Q., Yu, J., Miramontes, E., 2024. Sedimentary architecture of submarine lobes affected by bottom currents: Insights from the Rovuma Basin offshore East Africa. Basin Research 36, e12829. https://doi.org/10.1111/bre.12829.

Chen, Y., Yao, G., Wang, X., Lv, F., Shao, D., Lu, Y., Cao, Q., Tang, P., 2020. Flow processes of the interaction between turbidity flows and bottom currents in sinuous unidirectionally migrating channels: An example from the Oligocene channels in the Rovuma Basin, offshore Mozambique. Sedimentary Geology 404, 105680. https://doi.org/10.1016/j.sedgeo.2020.105680.

Corney, R.K.T., Peakall, J., Parsons, D.R., Elliott, L., Amos, K.J., Best, J.L., Keevil, G.M., Ingham, D.B., 2006. The orientation of helical flow in curved channels. Sedimentology 53, 249–257. https://doi.org/10.1111/j.1365-3091.2006.00771.x.

Cossu, R., Wells, M.G., 2010. Coriolis forces influence the secondary circulation of gravity currents flowing in large-scale sinuous submarine channel systems. Geophys. Res. Lett. 37. https://doi.org/10.1029/2010GL044296.

Cossu, R., Wells, M.G., Peakall, J., 2015. Latitudinal variations in submarine channel sedimentation patterns: the role of Coriolis forces. JGS 172, 161–174. https://doi.org/10.1144/jgs2014-043.

Covault, J.A., Fildani, A., Romans, B.W., McHargue, T., 2011. The natural range of submarine canyon-and-channel longitudinal profiles. Geosphere 7, 313–332. https://doi.org/10.1130/GES00610.1.

de Leeuw, J., Eggenhuisen, J.T., Cartigny, M.J.B., 2018a. Linking submarine channel–levee facies and architecture to flow structure of turbidity currents: insights from flume tank experiments. Sedimentology 65, 931–951. https://doi.org/10.1111/sed.12411.

de Leeuw, J., Eggenhuisen, J.T., Spychala, Y.T., Heijnen, M.S., Pohl, F., Cartigny, M.J.B., 2018b. Sediment volume and grain-size partitioning between submarine channel−levee systems and lobes: an experimental study. J. Sediment. Res. 88, 777–794. https://doi.org/10.2110/jsr.2018.46.

Einstein, H.A., Li, H., 1958. Secondary currents in straight channels. Trans. Am. Geophys. Union 39, 1085–1088. https://doi.org/10.1029/TR039i006p01085.

Ellison, T.H., Turner, J.S., 1959. Turbulent entrainment in stratified flows. J. Fluid Mech. 6, 423. https://doi.org/10.1017/S0022112059000738.

Falcini, F., Piliouras, A., Garra, R., Guerin, A., Jerolmack, D.J., Rowland, J., Paola, C., 2014. Hydrodynamic and suspended sediment transport controls on river mouth morphology. J. Geophys. Res. Earth 119, 1–11. https://doi.org/10.1002/2013JF002831.

Fonnesu, M., Palermo, D., Galbiati, M., Marchesini, M., Bonamini, E., Bendias, D., 2020. A new world-class deep-water play-type, deposited by the syndepositional interaction of turbidity flows and bottom currents: the giant Eocene Coral Field in northern Mozambique. Mar. Pet. Geol. 111, 179–201. https://doi.org/10.1016/j.marpetgeo.2019.07.047.

Fuhrmann, A., Kane, I.A., Clare, M.A., Ferguson, R.A., Schomacker, E., Bonamini, E., Contreras, F.A., 2020. Hybrid turbidite-drift channel complexes: an integrated multiscale model. Geology 48, 562–568. https://doi.org/10.1130/G47179.1.

Fuhrmann, A., Kane, I.A., Schomacker, E., Clare, M.A., Pontén, A., 2022. Bottom current modification of turbidite lobe complexes. Front. Earth Sci. 9, 752066. https://doi.org/10.3389/feart.2021.752066.

Galy, V., France-Lanord, C., Beyssac, O., Faure, P., Kudrass, H., Palhol, F., 2007. Efficient organic carbon burial in the Bengal fan sustained by the Himalayan erosional system. Nature 450, 407–410. https://doi.org/10.1038/nature06273.

Garcia, M.H., 1994. Depositional turbidity currents laden with poorly sorted sediment. J. Hydraul. Eng. 120, 1240–1263. https://doi.org/10.1061/(ASCE)0733-9429(1994)120:11(1240).

Gavey, R., Carter, L., Liu, J.T., Talling, P.J., Hsu, R., Pope, E., Evans, G., 2017. Frequent sediment density flows during 2006 to 2015, triggered by competing seismic and weather events: Observations from subsea cable breaks off southern Taiwan. Mar. Geol. Subaquat. Paleoseismol. 384, 147–158. https://doi.org/10.1016/j.margeo.2016.06.001.

Gong, C., Wang, Y., Rebesco, M., Salon, S., Steel, R.J., 2018. How do turbidity flows interact with contour currents in unidirectionally migrating deep-water channels? Geology 46, 551–554. https://doi.org/10.1130/G40204.1.

Gong, C., Wang, Y., Steel, R.J., Peakall, J., Zhao, X., Sun, Q., 2016. Flow processes and sedimentation in unidirectionally migrating deep-water channels: From a three-dimensional seismic perspective. Sedimentology 63, 645–661. https://doi.org/10.1111/sed.12233.

Hebbeln, D., Van Rooij, D., Wienberg, C., 2016. Good neighbours shaped by vigorous currents: Cold-water coral mounds and contourites in the North Atlantic. Mar. Geol. 378, 171–185. https://doi.org/10.1016/j.margeo.2016.01.014.
Heezen, B.C., Hollister, C.D., Ruddiman, W.F., 1966. Shaping of the continental rise by deep geostrophic contour currents. Science 152, 502–508. https://doi.org/10.1126/science.152.3721.502.
Henry, L.-A., Roberts, J.M., 2007. Biodiversity and ecological composition of macrobenthos on cold-water coral mounds and adjacent off-mound habitat in the bathyal Porcupine Seabight, NE Atlantic. Deep-Sea Res. I Oceanogr. Res. Pap. 54, 654–672. https://doi.org/10.1016/j.dsr.2007.01.005.
Hinsberger, R., Biehler, A., Yörük, A., 2022. Influence of water depth and slope on roughness—experiments and roughness approach for rain-on-grid modeling. Water 14, 4017. https://doi.org/10.3390/w14244017.
Hwang, H.G., Lee, J.H., 2018. Secondary flows in turbulent boundary layers over longitudinal surface roughness. Phys. Rev. Fluids 3, 014608. https://doi.org/10.1103/PhysRevFluids.3.014608.
Imamoto, H., Ishigaki, T., 1992. Flow visualization in a transverse cross section of an open-channel flow. Exp. Thermal Fluid Sci. 5, 268–273. https://doi.org/10.1016/0894-1777(92)90070-L.
Imran, J., Islam, M.A., Huang, H., Kassem, A., Dickerson, J., Pirmez, C., Parker, G., 2007. Helical flow couplets in submarine gravity underflows. Geology 35, 659–662. https://doi.org/10.1130/G23780A.1.
Kane, I.A., Clare, M.A., Miramontes, E., Wogelius, R., Rothwell, J.J., Garreau, P., Pohl, F., 2020. Seafloor microplastic hotspots controlled by deep-sea circulation. Science 368, 1140–1145. https://doi.org/10.1126/science.aba5899.
Keevil, G.M., Peakall, J., Best, J.L., Amos, K.J., 2006. Flow structure in sinuous submarine channels: velocity and turbulence structure of an experimental submarine channel. Mar. Geol. 229, 241–257. https://doi.org/10.1016/j.margeo.2006.03.010.
Kelly, R.W., Dorrell, R.M., Burns, A.D., McCaffrey, W.D., 2019. The structure and entrainment characteristics of partially confined gravity currents. J. Geophys. Res. Oceans 124, 2110–2125. https://doi.org/10.1029/2018JC014042.
Khripounoff, A., Crassous, P., Lo Bue, N., Dennielou, B., Silva Jacinto, R., 2012. Different types of sediment gravity flows detected in the Var submarine canyon (northwestern Mediterranean Sea). Prog. Oceanogr. 106, 138–153. https://doi.org/10.1016/j.pocean.2012.09.001.
Knight, D.W., Patel, H.S., 1985. Boundary shear in smooth rectangular ducts. J. Hydraul. Eng. 111, 29–47. https://doi.org/10.1061/(ASCE)0733-9429(1985)111:1(29).
McCave, I.N., Manighetti, B., Robinson, S.G., 1995. Sortable silt and fine sediment size/composition slicing: parameters for palaeocurrent speed and palaeoceanography. Paleoceanography 10, 593–610. https://doi.org/10.1029/94PA03039.
Miramontes, E., Garreau, P., Caillaud, M., Jouet, G., Pellen, R., Hernández-Molina, F.J., Clare, M.A., Cattaneo, A., 2019. Contourite distribution and bottom currents in the NW Mediterranean Sea: coupling seafloor geomorphology and hydrodynamic modelling. Geomorphology 333, 43–60. https://doi.org/10.1016/j.geomorph.2019.02.030.
Miramontes, E., Eggenhuisen, J.T., Jacinto, R.S., Poneti, G., Pohl, F., Normandeau, A., Campbell, D.C., Hernández-Molina, F.J., 2020. Channel-levee evolution in combined contour current–turbidity current flows from flume-tank experiments. Geology 48, 353–357. https://doi.org/10.1130/G47111.1.
Miramontes, E., Thiéblemont, A., Babonneau, N., Penven, P., Raisson, F., Droz, L., Jorry, S.J., Fierens, R., Counts, J.W., Wilckens, H., Cattaneo, A., Jouet, G., 2021. Contourite and mixed turbidite-contourite systems in the Mozambique Channel (SW Indian Ocean): link between geometry, sediment characteristics and modelled bottom currents. Mar. Geol. 437, 106502. https://doi.org/10.1016/j.margeo.2021.106502.
Mohrig, D., Buttles, J., 2007. Deep turbidity currents in shallow channels. Geology 35, 155–158. https://doi.org/10.1130/G22716A.1.
Nezu, I., Nakagawa, H., 1984. Cellular secondary currents in straight conduit. J. Hydraul. Eng. 110, 173–193. https://doi.org/10.1061/(ASCE)0733-9429(1984)110:2(173).
Pierdomenico, M., Casalbore, D., Chiocci, F.L., 2020. The key role of canyons in funnelling litter to the deep sea: a study of the Gioia Canyon (Southern Tyrrhenian Sea). Anthropocene 30, 100237. https://doi.org/10.1016/j.ancene.2020.100237.
Oertel, H. (Ed.), 2010. Prandtl-Essentials of Fluid Mechanics, Applied Mathematical Sciences. Springer, New York. https://doi.org/10.1007/978-1-4419-1564-1.
Pierdomenico, M., Bernhardt, A., Eggenhuisen, J.T., Clare, M.A., Lo Iacono, C., Casalbore, D., Davies, J.S., Kane, I., Huvenne, V.A.I., Harris, P.T., 2023. Transport and accumulation of litter in submarine canyons: a geoscience perspective. Front. Mar. Sci. 10. https://doi.org/10.3389/fmars.2023.1224859.
Pohl, F., Eggenhuisen, J.T., Tilston, M., Cartigny, M.J.B., 2019. New flow relaxation mechanism explains scour fields at the end of submarine channels. Nat. Commun. 10, 4425. https://doi.org/10.1038/s41467-019-12389-x.
Pohl, F., Eggenhuisen, J.T., Cartigny, M.J.B., Tilston, M.C., de Leeuw, J., Hermidas, N., 2020. The influence of a slope break on turbidite deposits: an experimental investigation. Mar. Geol. 424, 106160. https://doi.org/10.1016/j.margeo.2020.106160.
Pope, S.B., 2000. Turbulent Flows. Cambridge University Press, Cambridge, UK.
Rodrigues, S., Hernández-Molina, F.J., Kirby, A., 2021. A late cretaceous mixed (turbidite-contourite) system along the argentine margin: paleoceanographic and conceptual implications. Mar. Pet. Geol. 123, 104768. https://doi.org/10.1016/j.marpetgeo.2020.104768.
Rodrigues, S., Hernández-Molina, F.J., Larter, R.D., Rebesco, M., Hillenbrand, C.-D., Lucchi, R.G., Rodríguez-Tovar, F.J., 2022. Sedimentary model for mixed depositional systems along the Pacific margin of the Antarctic Peninsula: decoding the interplay of deep-water processes. Mar. Geol. 445, 106754. https://doi.org/10.1016/j.margeo.2022.106754.
Sánchez-Leal, R.F., Bellanco, M.J., Fernández-Salas, L.M., García-Lafuente, J., Gasser-Rubinat, M., González-Pola, C., Hernández-Molina, F.J., Pelegrí, J.L., Peliz, A., Relvas, P., Roque, D., Ruiz-Villarreal, M., Sammartino, S., Sánchez-Garrido, J.C., 2017. The Mediterranean Overflow in the Gulf of Cadiz: a rugged journey. Sci. Adv. 3, eaao0609. https://doi.org/10.1126/sciadv.aao0609.
Sequeiros, O.E., 2012. Estimating turbidity current conditions from channel morphology: a Froude number approach. J. Geophys. Res. Oceans 117. https://doi.org/10.1029/2011JC007201.
Sequeiros, O.E., Spinewine, B., Beaubouef, R.T., Sun, T., García, M.H., Parker, G., 2010. Characteristics of velocity and excess density profiles of saline underflows and turbidity currents flowing over a mobile bed. J. Hydraul. Eng. 136, 412–433. https://doi.org/10.1061/(ASCE)HY.1943-7900.0000200.
Shanmugam, G., Spalding, T.D., Rofheart, D.H., 1993. Process sedimentology and reservoir quality of deep-marine bottom-current reworked sands (sandy contourites): an example from the Gulf of Mexico. Bulletin 77. https://doi.org/10.1306/BDFF8E52-1718-11D7-8645000102C1865D.
Shiono, K., Knight, D.W., 1991. Turbulent open-channel flows with variable depth across the channel. J. Fluid Mech. 222, 617. https://doi.org/10.1017/S0022112091001246.
Simpson, J.E., 1972. Effects of the lower boundary on the head of a gravity current. J. Fluid Mech. 53, 759–768. https://doi.org/10.1017/S0022112072000461.
Sumner, E.J., Peakall, J., Dorrell, R.M., Parsons, D.R., Darby, S.E., Wynn, R.B., McPhail, S.D., Perrett, J., Webb, A., White, D., 2014. Driven around the bend: spatial evolution and controls on the orientation of helical bend flow in a natural submarine gravity current. J. Geophys. Res. Oceans 119, 898–913. https://doi.org/10.1002/2013JC009008.
Talling, P.J., Allin, J., Armitage, D.A., Arnott, R.W.C., Cartigny, M.J.B., Clare, M.A., Felletti, F., Covault, J.A., Girardclos, S., Hansen, E., Hill, P.R., Hiscott, R.N., Hogg, A.J., Clarke, J.H., Jobe, Z.R., Malgesini, G., Mozzato, A., Naruse, H., Parkinson, S., Peel, F.J., Piper, D.J.W., Pope, E., Postma, G., Rowley, P., Sguazzini, A., Stevenson, C.J., Sumner, E.J., Sylvester, Z., Watts, C., Xu, J., 2015. Key future directions for research on turbidity currents and their deposits. J. Sediment. Res. 85, 153–169. https://doi.org/10.2110/jsr.2015.03.
Talling, P.J., Hage, S., Baker, M.L., Bianchi, T.S., Hilton, R.G., Maier, K.L., 2024. The global turbidity current pump and its implications for organic carbon cycling. Annu. Rev. Mar. Sci. 16, 105–133. https://doi.org/10.1146/annurev-marine-032223-103626.
Wells, M., Cossu, R., 2013. The possible role of Coriolis forces in structuring large-scale sinuous patterns of submarine channel–levee systems. Philos. Trans. R. Soc. A Math. Phys. Eng. Sci. 371, 20120366. https://doi.org/10.1098/rsta.2012.0366.
Wilckens, H., Miramontes, E., Schwenk, T., Artana, C., Zhang, W., Piola, A.R., Baques, M., Provost, C., Hernández-Molina, F.J., Felgendreher, M., Spieß, V., Kasten, S., 2021. The erosive power of the Malvinas current: influence of bottom currents on morpho-sedimentary features along the northern argentine margin (SW Atlantic Ocean). Mar. Geol. 439, 106539. https://doi.org/10.1016/j.margeo.2021.106539.
Wilckens, H., Eggenhuisen, J.T., Adema, P.H., Hernández-Molina, F.J., Jacinto, R.S., Miramontes, E., 2023. Secondary flow in contour currents controls the formation of moat-drift contourite systems. Commun. Earth Environ. 4, 1–10. https://doi.org/10.1038/s43247-023-00978-0.
Xu, J.P., Noble, M.A., Rosenfeld, L.K., 2004. In-situ measurements of velocity structure within turbidity currents. Geophys. Res. Lett. 31. https://doi.org/10.1029/2004GL019718.
Zhao, Y., Liu, Z., Zhang, Y., Zhang, X., Ma, P., Yu, X., Ling, C., Lin, B., Zhang, J., 2024. Formation mechanism of drift-moat contourite systems revealed by in-situ observations in the South China Sea. Earth Planet. Sci. Lett. 628, 118585. https://doi.org/10.1016/j.epsl.2024.118585.